AIAA 94-0870

LIM Modeling of Chemical Reactions in Spatially and Temporally Developing Shear Flows

Nallan C. Suresh[2], Werner J.A. Dahm[1] and Grétar Tryggvason[2]

[1]Department of Aerospace Engineering
The University of Michigan
Ann Arbor, MI

[2]Dept. of Mechanical Engineering & Applied Mech.
The University of Michigan
Ann Arbor, MI

32nd Aerospace Sciences Meeting & Exhibit
January 10-13, 1994 / Reno, NV

LIM Modeling of Chemical Reactions in Spatially and Temporally Developing Shear Flows

Nallan C. Suresh, Werner J.A. Dahm and Grétar Tryggvason

Department of Aerospace Engineering
Department of Mechanical Engineering & Applied Mechanics
The University of Michigan, Ann Arbor, MI 48109

Abstract

A local integral moment (LIM) model is described for numerical calculations of flow structure, molecular mixing, and chemical reactions in complex flows. This physically-based formulation is based on the experimental, numerical, and theoretical observation that gradients of advected and diffused quantities concentrate into universal, self-similar, small-scale structures for large Peclet numbers *ReSc*. The model incorporates this self-similar structure at the diffusive scales directly through a local parabolization of the governing transport equations on a time-evolving material surface on which the gradients in the velocity and scalar fields are originally centered. These lead to equations governing local integral moments computed along the layer-normal direction at each point on the surface. This procedure effectively transforms the original set of partial differential equations that must be solved throughout a three-dimensional volume to a set of ordinary differential equations that can be solved on a two-dimensional surface. No closure approximations are required. The scalar and scalar dissipation fields are subsequently constructed from the integral moments on this surface, giving the local chemical species concentration fields via a strained diffusion and reaction layer formulation. The model is applied to three different test cases: molecular mixing in a laminar vortex pair, a one-step chemical reaction in a temporally developing shear layer, and mixing and complex chemical reaction by fuel injection into an enclosure. Results obtained in all three cases indicate that the model correctly retains the essential physics underlying such problems while bringing practical calculations of complex flows with complex chemistry within computational reach.

1. Introduction

Within the broad class of turbulent reacting flow problems, combustion processes in non-premixed reactant systems are among the most widely encountered. Applications range from combustor design in high speed airbreathing propulsion systems, to the reduction of environmental pollutants in industrial combustion systems. Issues of interest include comparatively simple questions such as the effect of confinement on flame geometry, to highly complex problems such as detailed predictions of potentially harmful trace species emissions produced by complex nonequilibrium reaction chemistry.

Direct numerical simulations (*DNS*) of turbulent flows, including molecular mixing and chemical reactions, have become possible within the last decade. However, severe computational restrictions are placed on these full simulations by the requirement that the entire range of spatial scales must be resolveable. In the case of chemically reacting flows, this includes the strain-limited diffusion scales arising in the vorticity field, where $\lambda_\nu \sim (\nu/\sigma)^{1/2}$, the species concentration fields, where $\lambda_D \sim (D/\sigma)^{1/2}$, and the chemical reaction rate fields, where for example $\lambda_R \sim \lambda_D\ (k/\sigma)^{1/3}$. In practice, these resolution restrictions limit the applicability of direct simulations to low Reynolds, Schmidt, and Damköhler numbers, to comparatively simple geometries, and to very simplistic chemical systems.

For this reason, classical models for dealing with turbulent flows and chemical reactions occurring within them have long been extensively used in practical problems. These models are essentially all based on the

time-averaged versions of the governing transport equations, and thus require classical *ad hoc* turbulence modeling of the gradient transport type to achieve closure. Even in nonreacting flows, the lack of physics in these models and their attendant shortcomings have long been recognized. Reacting flows present additional difficulties for such approaches. On the one hand, the time-averaged nature of these models precludes any accounting of the dynamical role played by large scale structures in setting the entrainment characteristics of turbulent shear flows. Moreover, even disregarding the consequent invalidity of the gradient transport treatment of turbulent flux terms, additional difficulties are encountered at the small scales in the treatment of the chemical reactions. The local instantaneous species production and consumption rates are set by elementary reactions rates given in terms of the *instantaneous* state of the chemical species and their respective mixing rates. As a consequence, the chemical source terms in these traditional models are notoriously difficult to relate back to the averaged quantities being solved.

A fundamentally different approach[1,2] to numerical simulation of detailed nonequilibrium reaction chemistry in complex turbulent flows has been under development over the past few years. Known as the local integral moment (LIM) method, this is a physically-based alternative that addresses many of the shortcomings of classical turbulence modeling approaches for reacting flows. A detailed description of the LIM model is given in §2. Briefly, this approach recognizes that the time evolution of large scales in the underlying turbulent flow must be computed explicitly in order to capture the flow-specific large scale structure. This is essential for obtaining the correct entrainment characteristics for the flow, and thereby setting the correct elemental environment for chemical reaction. As is the case in most reacting flow models, the LIM approach involves a separation of the molecular mixing and chemical reaction problems through a formulation in terms of one or more conserved scalar variables ζ. The advection-diffusion balance that governs the evolution of this scalar field leads to a universal self-similar layer-like structure at the small scales of the flow. The model incorporates this self-similar structure at the diffusive scales directly through a local parabolization of the governing transport equations on the time-evolving material surface on which the gradients in the scalar field are originally centered. This transforms the problem from an original set of *partial* differential equations that must be solved throughout the three-dimensional *volume* to a set of *ordinary* differential equations that can be solved on a two-dimensional *surface*. The diffusive scales in the vorticity transport equation are treated in the same way, thus freeing the numerical model from the need to resolve the diffusive scales directly, while still retaining the correct strain-diffusion competition that sets the small scales. The evolution of the scalar field then amounts to solving the resulting ordinary differential equations on the time-evolving material surface. The scalar field is then reconstructed from its integral moments on this surface, and from this the associated scalar dissipation rate field is also obtained. Since the scalar field statistics are essentially Reynolds number independent at values of Re above 10^4 or so, high Damköhler number calculations are possible by rescaling time in the scalar dissipation field while leaving the scalar field unchanged. The resulting joint scalar and scalar dissipation rate fields then allow arbitrarily complex reaction chemistry to be treated using the strained dissipation and reaction layer formulation[3,4,5]. This relates the local state of nonequilibrium reaction chemistry to the layer-like fine scale structure inherent in the dynamics of scalar mixing in turbulent flows. The resulting LIM model, while computationally far more demanding that traditional *ad hoc* turbulence models, is well within reach of current desktop computing workstations and appears able to accurately reproduce many physical characteristics of flow structure, molecular mixing, and chemcial reaction that are inaccessible to classical turbulence models and well beyond the reach of direct numerical simulations.

This paper summarizes the major features of the LIM model, and demonstrates its application to mixing and complex chemical reactions in two fundamentally different types of problems. The presentation is organized as follows. In Sec. 2 we give a detailed presentation of the LIM model, including its physical foundations, the derivation of the governing local integral equations, the scalar field reconstruction method, and the strained dissipation and reaction layer method for coupling the scalar field to the chemical species fields. Section 3 then presents sample results for mixing in a vortex pair, for which experimental and DNS data are available for comparison. Scalar and dissipation rate fields are presented both for large Sc mixing and for $Sc \approx 1$ scalars to demonstrate how the widely differing physical features are recovered by the LIM model. Section 4 applies the LIM equations for an explicit calculation of a single-step irreversible reaction with temperature-dependent Arrhenius kinetics in a reacting shear layer, and makes comparisons with direct numerical simulations of the same flow. In Sec. 5 we then present results for mixing and complex reaction chemistry in an enclosed chamber. The

resulting flow and the coupled chemistry far exceed the computational requirements of any direct simulation. Species concentration fields are presented from the LIM model, and effects of partial premixing are also demonstrated. We conclude in Sec. 6 with comments about the suitability of this LIM approach for approximately simulating complex nonequilibrium chemical reactions in complex flow fields for practical engineering calculations.

2. The LIM Model

2.1 *Physical Foundation*

Motivation and derivation of the LIM model are based on experimental results from detailed conserved scalar imaging measurements in nonreacting turbulent flows[6-10], as well as direct numerical simulations of passive scalar mixing in turbulent flows[11-15]. These show that, whereas the underlying hydrodynamics of turbulent flows are quite complex, the structure of scalar mixing in such flows is considerably simpler. For dynamically passive conserved scalar fields $\zeta(\mathbf{x},t)$ evolving at large Peclet ($ReSc$) numbers and Schmidt numbers of unity or larger, essentially all of the scalar energy dissipation rate field $(ReSc)^{-1}\nabla\zeta\cdot\nabla\zeta(\mathbf{x},t)$ is organized into locally one-dimensional layer-like dissipation sheets. The formation and evolution of these layer-like dissipation sheets are a consequence solely of the hydrodynamics of scalar mixing in turbulent flows. Recent results from conserved scalar imaging measurements[16] as well as DNS computations appear to confirm that these layer-like scalar dissipation structures remain present even in turbulent flows undergoing highly exothermic combustion reactions. Measurements[9] verify that the internal structure of these scalar dissipation layers are self-similar and essentially one-dimensional. As a consequence, spatial derivatives of the scalar field in the plane of the layer are small in comparison with the derivative along the layer-normal direction. Retaining only this normal derivative parabolizes the scalar transport equation, yielding a set of ordinary differential equations .

2.2 *The Local Integral Equations*

Any dynamically passive conserved scalar quantity $\zeta(\mathbf{x},t)$ satisfies the conservative advection-diffusion equation

$$\frac{\partial\zeta}{\partial t}+\mathbf{u}\cdot\nabla\zeta-\frac{1}{ReSc}\nabla^2\zeta=0 \qquad (1)$$

in which the dimensionless diffusivity is given by the product ($ReSc$) of the Reynolds and Schmidt numbers. For large Re and Sc of unity or larger, the Peclet number $ReSc$ associated with the diffusive term in (1) involves a singular limit that leads to the formation of internal "scalar gradient boundary layers." These scalar dissipation layers are the diffusive analog of the dissipation "shocks" that naturally form from the advection-diffusion balance high Reynolds number solutions of Burgers' equation. It is this advection-diffusion competition that leads to the formation and maintenance of the dissipation layers seen in conserved scalar imaging measurements as well as direct numerical simulations of scalar mixing. This same balance in the vorticity transport equation leads to localization of velocity gradients (internal intermittency) as well, however the vortex stretching term on the right side in that case allows both sheet-like and line-like vortical structures to be created. By comparison, in the scalar field the absence of such a source term precludes line-like structures, allowing only the formation of sheet-like dissipative structures. In both cases, the locally one-dimensional and self-similar structure within these vorticity and scalar dissipation layers allows development of computational methods that exploit this simplifying feature by incorporating it directly into the solution method, and thus alleviating many of the resolution difficulties classically associated with direct simulations of complex reacting flows.

Discarding spatial derivatives in all but the layer-normal direction n gives the parabolized form of the scalar transport equation in (1) as

$$\frac{\partial\zeta}{\partial t}-\sigma n\frac{\partial\zeta}{\partial n}-\frac{1}{ReSc}\frac{\partial^2\zeta}{\partial n^2}=0 \qquad (2)$$

where s is the local strain rate along n. Owing to the self-similarity of the scalar profiles within these layers, we define local integral moments G_j of all orders j for the scalar gradient profile across each layer as

$$G_j\equiv\int_{-\infty}^{+\infty}n^j\frac{\partial\zeta}{\partial n}dn,\quad j=0,1,2,\ldots \qquad (3)$$

The exact set of transport equations for these moments can be readily derived from (2), giving ordinary differential equations (ODE's) for the time-evolution of the local moments as

$$\frac{dG_0(s)}{dt}=0 \qquad (4a)$$

$$\frac{dG_1(s)}{dt}=-\sigma(s)G_1(s) \qquad (4b)$$

$$\frac{dG_2(s)}{dt} = -2\sigma(s)\,G_2(s) - \frac{2}{ReSc}G_0(s) \quad (4c)$$

$$\vdots$$

where the coordinate s identifies the location along the layer. These local integral moment equations are exact. The infinite set of ODE's for these integral moments G_j for $j = \{1, \ldots, \infty\}$ are completely equivalent to the partial differential equation (PDE) in (2). However, owing to the linearity of the one-dimensional strained diffusion equation in (2), these local integral moment equations have the property that they are exactly closed at any level of truncation of the infinite set. In other words, the set of equations for the integral moments G_j for $j = \{1, \ldots, k\}$ involves only the moments G_j of order k and lower. As a result, the time evolution of the local moments up to any desired order can be exactly determined from the local integral equations.

Note that this approach is somewhat similar in principle to various integral methods based on the von Karman boundary layer integral equation in boundary layer theory, wherein a family of shapes for the velocity profile in the boundary layer is assumed, and the integral equation determines the global properties such as wall shear stress or layer thickness. Here the objective is instead to determine the internal structure of the scalar gradient layer embedded in a complex time-evolving flow field.

For the scalar gradient field, the solution involves numerically integrating the time-evolution of the integral moments G_j everywhere on the material surface on which the scalar gradients are concentrated by the initial and boundary conditions. The scalar field evolution is coupled to the velocity field through the local strain rate σ in (4), which is determined from the deformation rate at each point on this material surface. The material surface itself evolves from the Biot-Savart induced velocities resulting from the vorticity in the flow field calculation, namely

$$\mathbf{u}(\mathbf{x},t) = \int_{\mathbf{x}'} \omega(\mathbf{x}',t) \times \frac{\mathbf{x}-\mathbf{x}'}{|\mathbf{x}-\mathbf{x}'|^3}\, d^3\mathbf{x}' \quad (5)$$

The localized vorticity concentrations that result from the advection-diffusion balance in the vorticity transport equation

$$\frac{\partial \omega}{\partial t} + \mathbf{u}\cdot\nabla\omega - \frac{1}{Re}\nabla^2\omega = \omega\cdot\nabla\mathbf{u} \quad (6)$$

allow a similar local integral treatment in the flow field calculation that underlies the solution of (4). This leads to a set of analogous local integral equations for the moments Γ_j for $j = \{1, \ldots, \infty\}$. For simplicity, we presently track only the zeroth integral moment in this set, which then satisfies a similar equation as in (4*a*), namely

$$\frac{d\Gamma_0(s)}{dt} = 0 \quad (7)$$

where $\Gamma_0(s)$ is the zeroth moment of the local vorticity profile (i.e. the local circulation density). Since (7) simply demands that the circulation associated with material points remains constant with time, solution of the integral moment equation in (7) can be achieved via a vortex-in-cell implementation for given initial and boundary conditions.

At every time t, the vorticity field from (7) produces the velocity field via (5), which then is used to advect each point s on the material surface over the next time step. The relative displacements of neighboring points on this surface then give the strain rate σ at each point on the material surface. The local strain rate $\sigma(s)$ then drives the evolution of the scalar gradient moments at that point via (4). In this manner, the time evolution of the integral moments for the scalar gradient field at each point on the evolving material surface are computed. The scalar field and associated scalar dissipation field are then constructed from the resulting distribution of integral moments over the surface following the procedure outlined in §2.3.

2.3 *Scalar Field Reconstruction*

The distribution of local integral moments $G_j(s)$ over the computational surface can be used to construct the scalar field $\zeta(\mathbf{x},t)$ throughout any volume of interest by a procedure outlined in this section. We use a simple family of self-similar profile shapes described by, say, k independent parameters (degrees of freedom) to model the local scalar gradient profile along the layer-normal direction n. Tracking the first k integral moments $G_j(s)$ then determines the local gradient profile. This allows the scalar gradient field $\nabla\zeta(\mathbf{x},t)$ to be evaluated at each point on a grid chosen for the scalar field construction. We then numerically evaluate the divergence $\nabla\cdot\nabla\zeta(\mathbf{x},t)$ of the resulting scalar gradient field on this grid. This (known) gradient divergence field is then used as the right hand side in the definition of the Laplacian of the scalar field, namely

$$\nabla^2\zeta = \nabla\cdot\nabla\zeta(\mathbf{x},t) \quad (8)$$

The Poisson equation in (8) is then solved for the known right hand side to give the scalar field $\zeta(\mathbf{x},t)$.

Solution of (8) requires boundary conditions for the region of interest in which the scalar field is to be constructed from its gradient moments. Owing to the very fine spatial scales present in the scalar field, we generally perform this reconstruction procedure on a sequence of successively finer grids to "zoom in" on any section of interest in the flow. The procedure described above is first performed on a coarse grid bounded by solid walls enclosing the entire flow field, for which the physically appropriate zero scalar flux requirement provides the necessary boundary conditions in (8). The requisite zero scalar gradient normal to the wall is implemented by a method of images. The resulting solution on the coarse grid then provides the scalar field values on boundaries of smaller domains in the interior of the flow. These boundary values in turn allow (8) to be solved in each of the smaller domains. Refined constructions of the scalar field in any selected domain in the flow can be obtained by subsequent repetitions of this procedure on increasingly smaller domains. For the results presented in Sec. 4, six grid refinements sufficed to provide the scalar field with essentially full spatial resolution.

The resulting scalar field $\zeta(\mathbf{x},t)$ is then differentiated on the final grid to obtain the scalar dissipation rate field $\nabla\zeta\cdot\nabla\zeta(\mathbf{x},t)$. The joint scalar and scalar dissipation information at each point is then used construct the chemical species field following the procedure outlined in §2.4.

2.4 *Chemical Species Fields*

Consistent with the layer-like foundation of the LIM method used here to obtain the scalar field and its time evolution, we use the strained dissipation and reaction layer formulation[3-5] to related the chemical species concentration and reaction rate fields to the scalar and scalar dissipation field resulting from the procedure in §2.3. The procedure for doing this is outlined in detail in Ref. 5. Here we summarize the essential aspects of the method.

The fundamentally layer-like structure of scalar mixing in turbulent flows on which the LIM method is based, as outlined in Sec. 1 and in §2.1, has far-reaching implications for turbulent combustion. As noted earlier, these dissipation layers result entirely for hydrodynamical reasons. Thus all conserved scalar quantities with $Sc \geq 1$ must have their scalar energy dissipation concentrated in such locally one-dimensional layer-like structures. This will be true irrespective of whether the scalar is a passive physical quantity, or a more abstract quantity such as any of various mixture fraction variables formed from the concentrations of various chemical species evolving in the flow. Moreover, since this is a consequence solely of the hydrodynamics of scalar mixing, the layer-like structure must be preserved irrespective of the degree of chemical nonequilibrium to which the various constituent chemical species fields are subjected. This inherently layer-like structure of the dissipation rate fields associated with mixture fraction variables in turbulent reacting flows provides a rigorous starting point for models of nonequilibrium chemistry in turbulent flows.

The strained dissipation and reaction layer model begins with the fact that any conserved scalar mixture fraction variable ζ_i can be written as a linear sum over the chemical species fields $Y_j(\mathbf{x},t)$ as

$$\zeta_i(\mathbf{x},t) = \sum_{j=1}^{N} a_{i,j} Y_j(\mathbf{x},t) \qquad i = 1,2,\ldots,m \qquad (9)$$

where N is the number of chemical species and m the number of elements involved in the chemical system. Owing to the locally one-dimensional structure of the scalar field within any given dissipation layer, each of these conserved scalars ζ_i in (9) must satisfy a locally one-dimensional advection-diffusion equation similar to that in (2). Note that, as is typically the case in conserved scalar formulations, we are for the moment treating the diffusivities of all species as being the same. In general the scalar dissipation layers in turbulent flows do not involve pure fuel or pure air on either side of the layer, and thus the correct *local* boundary conditions for these equations can be expressed as $\zeta_i \rightarrow \zeta_i^{\pm}$ as $n \rightarrow \pm\infty$. Replacing the ζ_i's in (2) with their definitions in terms of the chemical species fields in (9) then leads to locally one-dimensional advection-diffusion-reaction equations for the chemical species fields $Y_j(\mathbf{x},t)$. In other words, the one-dimensionality of the local conserved scalar field across each strained dissipation layer implies a locally one-dimensional structure for the underlying chemical species fields within the layer, though owing to the local boundary conditions on (10) this does not imply that the resulting $Y_j(\mathbf{x},t)$ fields must be layer-like. The (steady) solutions $Y_j(n;\sigma)$ to these equations can be equivalently given as libraries of $Y_j(\zeta,\nabla\zeta\cdot\nabla\zeta;\ \zeta^{\pm})$ from the solution for ζ in (2). The scalar and scalar dissipation values thus determine the local chemical composition at each point in the flow.

Note that this is precisely the opposite view from that usually taken in deriving the classical "flamelet" model. In the flamelet model, conditions are assumed for which the flamelet is thin, and the species transport equations then formally reduce to locally one-

dimensional equations which, in turn, dictate a locally one-dimensional structure in the mixture fraction fields $\zeta_j(\mathbf{x},t)$. However, the conditions under which this thin flamelet assumption holds are so restrictive that the flamelet model is useful only for small equilibrium departures. By comparison, the strained dissipation and reaction layer model begins with the physical observation that the mixture fraction fields $\zeta_j(\mathbf{x},t)$ in turbulent flows must be locally one-dimensional, and argues that this requires the constituent chemical species fields $Y_j(\mathbf{x},t)$ to also be locally one-dimensional. However, unlike the flamelet model, the resulting one-dimensionality in this case does not demand thin "flamelet-like" $Y_j(\mathbf{x},t)$ fields – the thinness requirement to which flamelet models are subject is not a constraint here. The resulting strained dissipation and reaction layer model thus has certain resemblances to the classical "flamelet" model, but is based on entirely different physical observations, is derived from entirely different arguments, and is limited by an entirely different and more widely applicable set of conditions. Moreover, the *local* boundary conditions for the one-dimensional advection-diffusion-reaction equations within any given dissipation layer differ fundamentally from classical flamelet models.

It is shown in Ref. [5] that the strained dissipation and reaction layer model is inherently capable of producing thin (flamelet-like) mass fraction and reaction rate fields under conditions of relatively weak chemical nonequilibrium, and the natural emergence and dominance of broad (distributed) species concentration and reaction rate fields for increasing chemical equilibrium departures. This formulation thus provides a physical and theoretical framework that reconciles these two widely disparate views of the coupling of the underlying fluid dynamics to the reaction chemistry in turbulent combustion within a single model. The layer-like scalar dissipation structures at the core of the LIM approach, together with this strained dissipation and reaction layer formulation, suffice to account for both the "flamelet" and "distributed" combustion regimes under differing conditions of nonequilibrium and locations in the flow.

3. Vortex Ring Mixing Test

In this section, we apply the LIM model as formulated in Sec. 2 to the molecular mixing process in a relatively simple flow, namely a laminar vortex pair. The well documented features of mixing in this simple flow permit qualitative validation of the model results. Results obtained for the conserved scalar and scalar dissipation rate fields are presented in Fig. 1 for two different values of the Peclet number ($ReSc$). In the top row of panel in this figure, the Peclet number is 150, corresponding for instance to either a gaseous ($Sc \approx 1$) scalar quantity diffusing in a $Re \approx 150$ vortex pair, or equivalently to a higher Sc scalar in a lower Re vortical flow. At the bottom the Peclet number is 2000, which corresponds for example to a lower diffusivity ($Sc \approx 13$) scalar in the same $Re \approx 150$ vortex pair, or equivalently to the $Sc \approx 1$ gaseous scalar in a $Re \approx 2000$ vortex pair.

In each case, the material surface on which the integral moments equations in (4) are solved is shown at the instant for which the scalar field is given. The differences in the two cases shown result entirely from the differing values of the Peclet number. In particular, note that whereas the material interface in both cases has the clearly rolled up structure expected for a vortex pair, essentially all evidence of this structure in the scalar field has been smeared out by molecular diffusion in the lower Peclet number case. This can be verified by the corresponding scalar dissipation field in the top row, where little evidence of any layered roll-up structure can be seen. This is in good agreement with scalar imaging measurements of gaseous mixing in low Reynolds number vortex flows, which show structure similar to that in seen in the center panel. By comparison, in the higher Peclet number case, there is a clear rolled-up layer structure evident in both the scalar and scalar dissipation fields in the bottom row. This too is in good agreement with imaging measurements of scalar mixing in liquid vortex flows, for which the Schmidt number is large and thus the Peclet number typically also large. Overall the features evident in these two cases appear to accurately reflect the changes in structure with Peclet number for molecular diffusion in vortical flows.

Finally, note that solution for the integral moments on the computational surface from (4) in both these cases is equally simple. In contrast, direct numerical simulations of mixing in fluid flows typically become increasingly more time-consuming as gradients in the solution become steeper with increasing Peclet number. This ultimately sets the limitations on Reynolds, Schmidt and Damköhler numbers accessible by direct numerical simulations, as discussed in Sec. 1. By comparison, in these LIM calculations the computational time required is independent of the fluid parameter values. Thus even mixing flows with very steep gradients, the time evolution of the integral moments can be tracked with no greater difficulty than for flows with relatively smooth gradients. It is therefore at the high parameter values typical of most practical problems that the LIM model is expected to be

of greatest use, where direct numerical simulations are clearly impossible, and where classical approaches for modeling turbulent mixing are too thinly rooted in the relevant fluid physics to progress much beyond their current shortcomings.

4. Reacting Shear Layer Results

Before demonstrating application of the LIM model to molecular mixing and detailed reaction chemistry in a complex flow, for which no direct numerical simulations are possible for comparison, we examine a simpler case for which DNS calculations are possible. In particular, we will consider a shear layer in which a single-step, irreversible reaction with temperature-dependent Arrhenius kinetics occurs between the two fluid streams. The implementation of the LIM method in this case is essentially the same as given in Sec. 2, except that the chemical species fields are evolved explicitly rather than by the strained dissipation and reaction layer library approach outlined in §2.4. The integral moments of the chemical species fields are evolved on the material surface obtained from the direct simulation via local integral moment equations otherwise analogous to those in (4). The flow is a temporally developing two-dimensional shear layer perturbed in its fundamental mode, leading to formation and rollup of a single vortical structure in which the reaction occurs. The calculations are for $Re = 2000$ and $Sc = 1$ at two different values of the Damköhler number. The first, corresponding to $Da = 30$, is for a sufficiently slow chemical reaction that local extinction occurs in the braids between the vortices. In the second case $Da = 300$, corresponding to faster chemistry for which reaction is maintained throughout the flow.

A detailed presentation of results from these cases can be found in Ref. 1. In Fig. 2 we show typical results obtained for both Damköhler numbers from the direct simulation and the LIM model. In this case, the fields shown give one of the reactant concentrations for nine equally spaced contours between ranging between pure fuel and pure oxidizer. The top two rows of panels in this figure compare the direct simulation and model results at $Da = 30$, while the two bottom rows compare the resulting fields from the simulation and the LIM model for the $Da = 300$ case. Note that in each case, the LIM model results are remarkably similar to those from the direct simulation. This is true despite the fact that the reactant concentration field shown differs substantially at these two different Da values. In the top case, fuel remains present throughout the vortex core, whereas in the two lower rows the fuel is cunsumed through much of the interior of the vortical structure. The LIM model predicts these differences rather well. In fact, the more extensive results presented in Ref. 1 demonstrate that the detailed spatial and temporal structure in all the concentration and reaction rate fields, as well as the temperature field, are accurately predicted by the LIM model. Even the highly nonlinear local extinction in the vortical braids is well reproduced. The good agreement obtained for these two widely differing cases is all the more remarkable in view of the fact that there are *no* adjustable parameters in the LIM model.

Note that the Reynolds, Schmidt and Damköhler numbers in this case are necessarily low to permit direct numerical simulations for validation of the LIM results. In the following section, a complex turbulent flow in which a relatively detailed set of chemical reactions occurs is simulated via the LIM model. In that case, direct simulations for comparison are far beyond computational reach. However, based on the results obtained in this reacting shear layer test case, and those obtained in Sec. 3 for mixing in the vortex flow at widely differing Peclet numbers, it appears possible to conclude that the LIM model is capable of accurately tracking the flow field and mixing processes at parameter values that are outside the range of direct simulations.

5. Complex Reacting Flow Results

In this section we demonstrate application of the LIM method in Sec. 2 to model the fluid flow, molecular mixing, and chemical reaction in a relatively complex flow. For this case, the reaction chemistry is sufficiently complex to preclude explicit calculation of the species fields from separate LIM equations of the type in (4). Instead, we implement the complex chemistry scheme via the strained dissipation and reaction layer library approach outlined in §2.4.

5.1 *Geometry*

The flow in this case simulates the mixing of a two-dimensional fuel jet in a small enclosure with an inflow of oxidizer through the front wall and an outflow at the back wall. The inflow and outflow are specified by source and sink distributions, with the remaining walls of the enclosure satisfying zero flux boundary conditions. The fuel injector is modeled by introducing vorticity in a manner satisfying zero flux through the injector walls and the Kutta condition to simulate separation at the end of the injector slot. Zeroth order moments are tracked for the vorticity, and moments of first and second order are tracked for the scalar gradient using a Peclet number of 5,000. The resulting scalar

dissipation field is then rescaled as discussed in Sec. 1 to *ReSc* numbers of 50,000 and 500,000.

The material surface (line) on which the integral moments for the vorticity and scalar gradients are tracked originally emanates from the lip of the injector slot. The points defining this surface are subsequently evolved in a Lagrangian fashion, with redistribution after every 20 time steps used to maintain adequate definition of the surface throughout the calculation. During this redistribution, vorticity and scalar gradient points are also removed (and their dynamical content distributed to neighboring points) on those parts of the interface that have become dynamically irrelevant. This procedure allows control over the number of points that are tracked by the model calculation. For the redistribution parameters used here, once the evolution of the material interface has reached an essentially steady state, the surface contains roughly 16,000 Lagrangian points. The surface is shown in this essentially steay state stage of its development in Fig. 3.

5.2 *Scalar Field Results*

The scalar field construction at any desired time step in the calculation is performed using the procedure described in §2.3 from the integral moments computed on the time-evolving material surface for the initial and boundary conditions described in §4.1. This construction begins on a 160×64 grid and proceeds via successive refinements as outlined above. The final grid consists of 18 sections, each with a resolution of 240×240 points, so that there are a total of 1,036,800 points defining the scalar field in the interior of the enclosure. An example of the scalar field $\zeta(\mathbf{x},t)$ for $ReSc = 5{,}000$ is shown in Fig. 4 at the same time at which the material interface was shown in Fig. 3.

Figure 5 shows profiles of various turbulent transport terms in the velocity and scalar fields obtained from the LIM model calculations at two different downstream locations in the flow. At the x/L = 20 location, where L is the injector slot width, the flow is still sufficiently far from the enclosure walls that we can expect these profiles to qualitatively agree with turbulence measurements from the self-similar far field of planar turbulent jets. There are numerous such measurements reported in the literature, and it can be seen that the profile shapes agree relatively well with these. For instance, the mean square axial fluctuation profile shows the characteristic dip near the centerline, and the peak value is in reasonable agreement with measurements. The same is true for the scalar variance profile. The mean square lateral fluctuation profile also has roughly the shape seen in measurements, but the peak fluctuation level is of course much higher owing to the strict two-dimensionality of the present model calculation. Nevertheless, the Reynolds stress profile and the turbulent transport profiles for the scalar field all have roughly the correct shape at this downstream location. At the x/L = 35 location, the influence of the walls should be significant. The flow would thus no longer be expected to follow the self-similar profiles applicable at the earlier location, and this is verified by the model results.

Classical "turbulence" profiles of the type in Fig. 5 are common in turbulence lore, but are themselves not particularly insightful nor relevant to the major objectives of turbulent reacting flow models. Instead, these models aim to predict the chemical species fields within the flow, and turbulence profiles of this type are at best indirectly related to that goal. In the following section, we use instantaneous scalar fields of the type in Fig. 4 resulting from the LIM model to directly construct the chemical species fields using the strained dissipation and reaction layer formulation outlined in §2.4.

5.3 *Chemical Species Fields*

Differentiation of scalar fields $\zeta(\mathbf{x},t)$ of the type in Fig. 4 allow direct evaluation of the scalar energy dissipation rate field $\nabla\zeta\cdot\nabla\zeta(\mathbf{x},t)$. Figure 6 shows the scalar dissipation field obtained from the scalar field in Fig. 4. Simultaneous knowledge of these two fields allows direct construction of chemical species concentration and reaction rate fields, as well as the temperature and heat release rate fields, throughout the flow. This involves the library approach based on the underlying layer-like structure in the dissipation field and its implications for locally one-dimensional structure in the chemical species transport equations, as discussed above.

Here we present results for several species in a reduced methane-air kinetic mechanism for two different nozzle fluid compositions. The first corresponds to pure methane ($\zeta = 1$) issuing from the injector, while the second corresponds to a partially premixed combination of methane and air ($\zeta = 0.15$) being injected into the enclosure. These nozzle fluid ζ values simply rescale the entire $\zeta(\mathbf{x},t)$ field, however the shift that this introduces in the location of the *instantaneous* stoichiometric contour in the resulting scalar field produces large changes in the resulting chemical species fields, as can be seen in the results in Figs. 7-11.

The depth of chemical nonequilibrium is controlled by the scalar dissipation rates. As noted in Sec. 1, for conditions at which the scalar field statistics have become essentially independent of the Reynolds number (typically by values of the order of 10^4 or so for most shear flows), the effects of further increases in *Re* lead primarily to smaller spatial scales in the scalar field and higher scalar dissipation rates. If the latter effect is dominant in controlling the effects this has on the depth of chemical nonequilibrium, then the higher Damköhler numbers can be accounted for by a simple rescaling of the scalar dissipation rates. This is done here to map the scalar dissipation field to effective Peclet numbers of 50,000 and 500,000, for which significant nonequilibrium chemistry effects can be seen in the resulting chemical species fields.

Figure 7 shows the methane concentration field for the non-premixed case at $ReSc$ = 500,000 and for the partially premixed case at $ReSc$ = 50,000. Non-equilibrium chemistry effects are small in major species like CH_4, and thus the major differences between the two cases result from the partial premixing. Note that, even in the partially premixed case, raw methane is seen to exit the relatively short combustion chamber through the duct at the back wall. OH radical concentration fields are shown for these two cases in Fig. 8. In the nonpremixed case, the relatively fuel rich concentration field suggests that OH appears in only thin zones within the flow, as compared with the partially premixed case where the shift in stoichiometric contour shows broader OH zones despite the lower dissipation rates. Similar results are shown for O-atom concentrations in Fig. 9, CO concentration in Fig. 10, and the temperature gradients in Fig. 11.

6. Conclusions

Results of the type presented here demonstrate the relatively detailed insights into chemically reacting flows attainable with a physically-based local integral moment model of the type developed here. Such views of reacting flows are potentially capable of contributing to an improved understanding of combustion processes in practical devices, especially when both the flow field and the reaction chemistry in them are beyond the reach of any direct simulations, and outside the regime in which traditional turbulent combustion models are deemed reliable. However, while validation test cases of the type in Secs. 3 and 4, as well as more extensive validations in Refs. 1-5, provide strong indications that the model results retain the essential physics important in problems of this type, further validations for complex flows and complex chemistry are needed to establish the validity of this new modeling approach.

Acknowledgements

This work is being supported by the Gas Research Institute (GRI) under GRI Contract No. 5088-260-1692. Discussions with Robert Krasny in the Applied Mathematics group at Michigan are gratefully acknowledged, as is the assistance of Mr. Chester Chang in developing the scalar field construction method.

References

1. Chang, C.H.H., Dahm, W.J.A. & Tryggvason, G. (1991) Lagrangian model simulations of molecular mixing, including finite rate chemical reactions, in a temporally developing shear layer. *Phys. Fluids A* **3**, 1300.

2. Tryggvason, G. & Dahm, W.J.A. (1990) An integral method for mixing, chemical reactions, and extinction in unsteady strained diffusion layers. *Comb Flame* **83**, 207.

3. Dahm, W.J.A. and Bish, E.S. (1993) High resolution measurements of molecular transport and reaction processes in turbulent combustion. Turbulence and Molecular Processes in Combustion, (T. Takeno, Ed.) 287, Elsevier Science Publishers B.V.

4. Bish, E.S., Dahm, W.J.A. & Dowling, D.R. (1993) A strained dissipation and reaction layer formulation for turbulent diffusion flames; Paper No. 93-063, 1993 Fall Meeting of the Western States Section of the Combustion Institute, Pittsburgh.

5. Bish, E.S. & Dahm, W.J.A. (1994) Nonequilibrium structure of H_2-air combustion in turbulent jets. Paper No. 94-0100, 32nd Aerospace Sciences Meeting, AIAA, Washington, D.C.

6. Dahm, W.J.A. & Buch, K.A. (1991) High resolution, three-dimensional (2563), spatio-temporal measurements of the conserved scalar field in turbulent shear flows; Turbulent Shear Flows 7, pp. 17–26, W.C. Reynolds, Ed., Springer Verlag, Berlin.

7. Dahm, W.J.A., Southerland, K.B. & Buch, K.A. (1991) Four-dimensional laser induced fluorescence measurements of conserved scalar mixing in turbulent flows; Applications of Laser Techniques to Fluid Mechanics, pp. 3–18, R. Adrian, Ed., Springer Verlag, Berlin.

8. Dahm, W.J.A., Southerland, K.B. & Buch, K.A. (1991) Direct, high resolution, four-dimensional measurements of the fine scale structure of Sc » 1 molecular mixing in turbulent flows; Phys. Fluids A 3, 1115-1127.

9. Buch, W.J.A. & Dahm, W.J.A. (1992) Fine scale structure of conserved scalar mixing in turbulent shear

flows: Sc » 1, Sc = 1 and implications for reacting flows; University of Michigan Report No. 026779-5, The University of Michigan, Ann Arbor, MI.

10. Buch, K.A., Dahm, W.J.A., Dibble, R.W. & Barlow, R.S. (1992) Equilibrium structure of reaction rate fields in turbulent diffusion flames; Proc. 24th Symp. (Int'l.) on Comb. 295-301, The Combustion Institute, Pittsburgh.

11. Siggia, E.D. (1981) Numerical study of small scale intermittency in three-dimensional turbulence. *J. Fluid Mech.* **107**, 375-406.

12. Kerr, R.M. (1985) Higher-order derivative correlations and the alignment of small scale structures in isotropic numerical turbulence; J. Fluid Mech. 153, 31-58.

13. Reutsch, G.R. & Maxey, M.R. (1991) Small-scale features of vorticity and passive scalar fields in homogeneous isotropic turbulence; Phys. Fluids A 3, 1587-1597.

14. Mell, W., Kosály, G. & Riley, J.J. (1993) An investigation of closure models for nonpremixed turbulent reacting flows; AIAA Paper No. 93-0104, AIAA, Washington, D.C.

15. Montgomery, C.J., Kosály, G. & Riley, J.J. (1993) Direct numerical simulation of turbulent H2–O2 combustion using reduced chemsitry; AIAA Paper No. 93-0248, AIAA, Washington, D.C.

16. Long, M.B. (1993) Proceedings of the 1993 AFOSR Contractors Meeting in Propulsion, AFOSR, Washington, D.C.; also private communication.

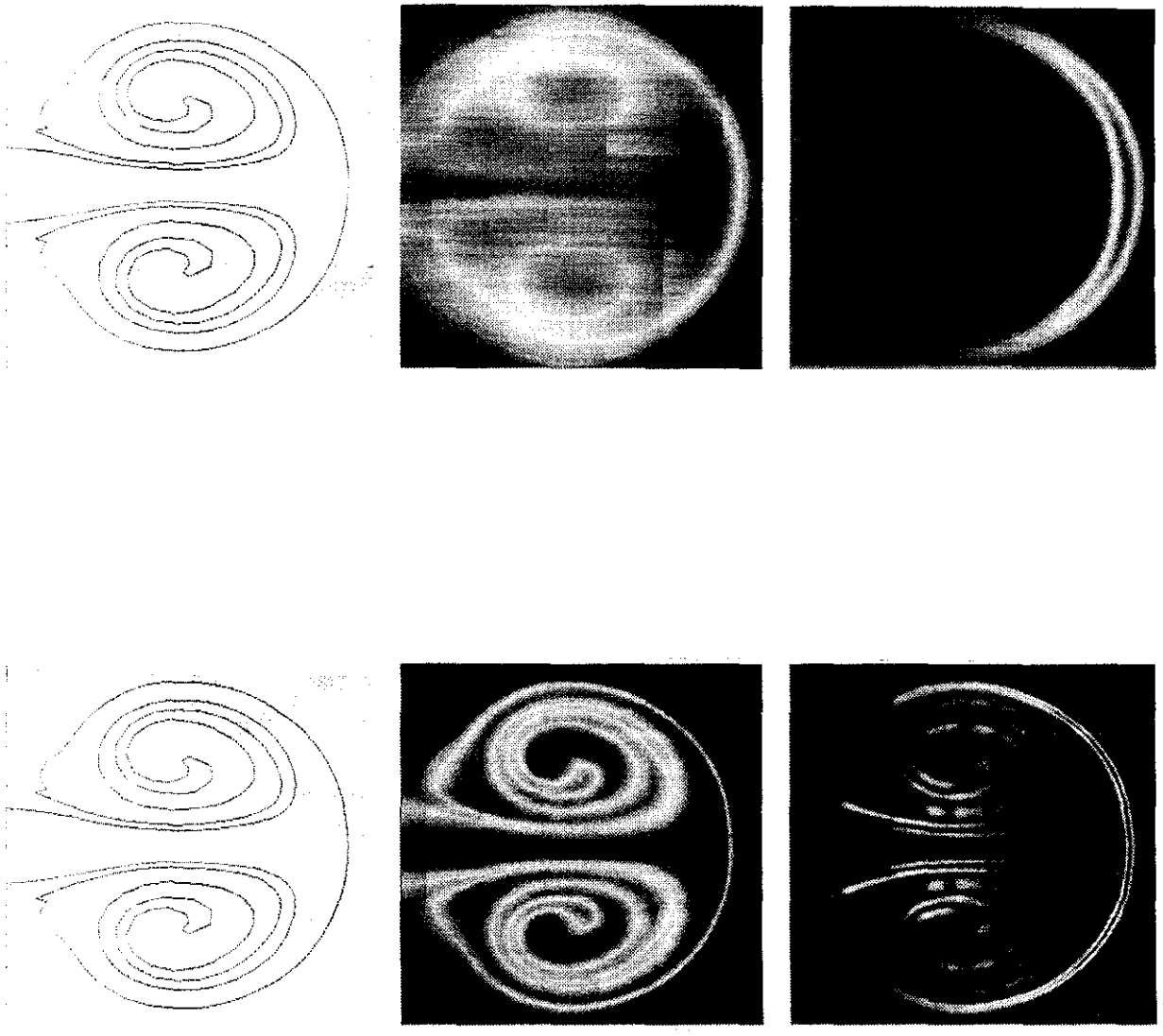

Fig. 1. Material front (left), scalar field (center) and scalar dissipation rate field for a 2-D jet emerging from a nozzle(ReSc=150 [top], 2000 [bottom])

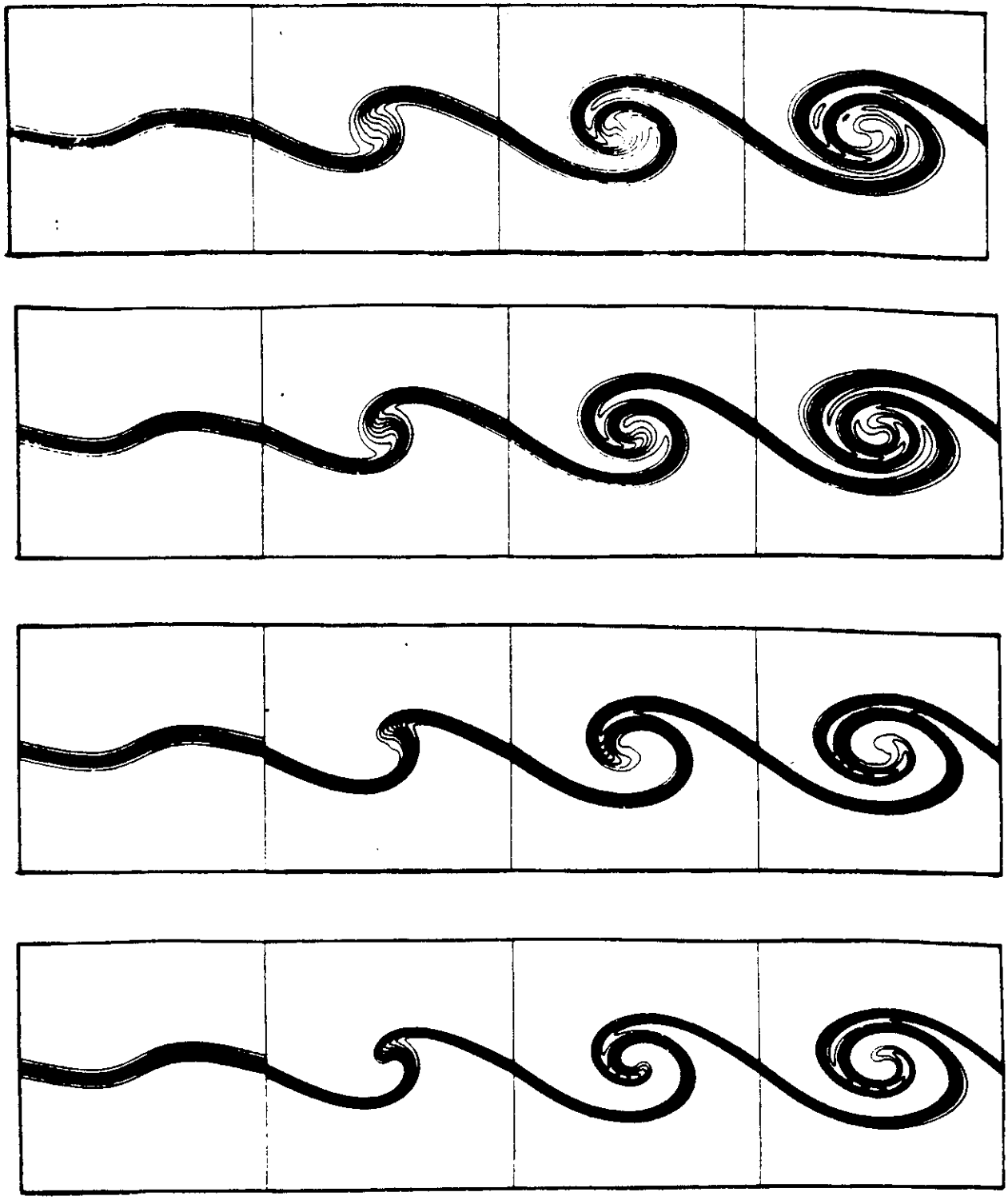

Fig. 2 LIM model and full finite difference simulation results using the explicit reaction integral, showing the scaled reaction concentration field. From top to bottom: (a) LIM model results (Re=2000, Da=30); (b) Finite difference results (Re=2000, Da=30); (c) LIM model results (Re=2000, Da=300); (d) Finite difference results (Re=2000, Da=300). [Chang, Dahm and Tryggvason(1991)]

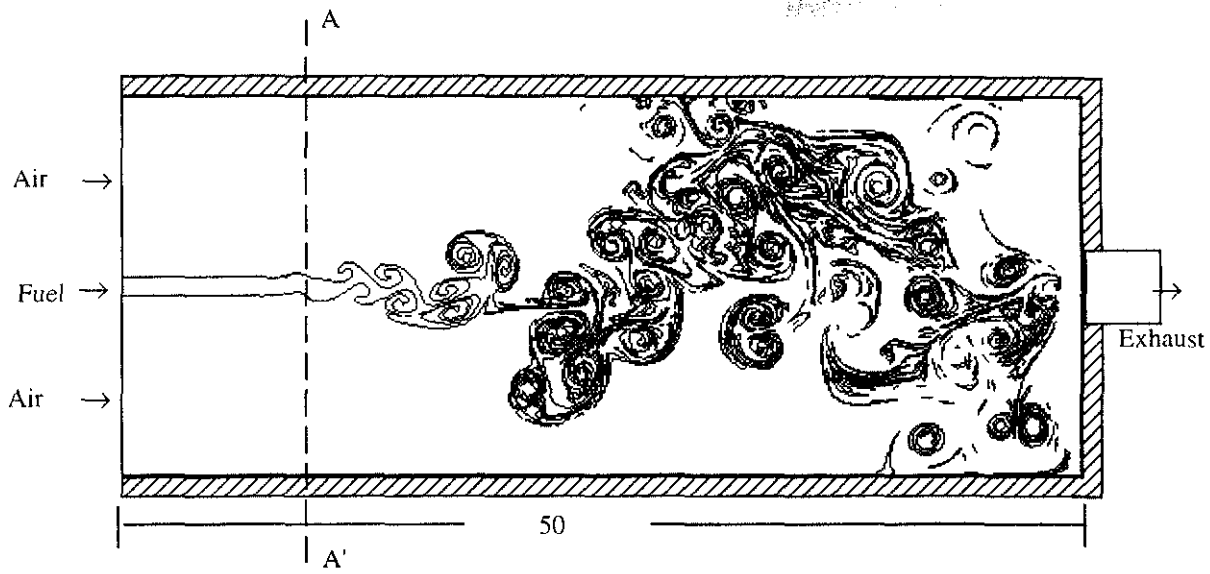

Fig. 3. Material interface evolution at large time

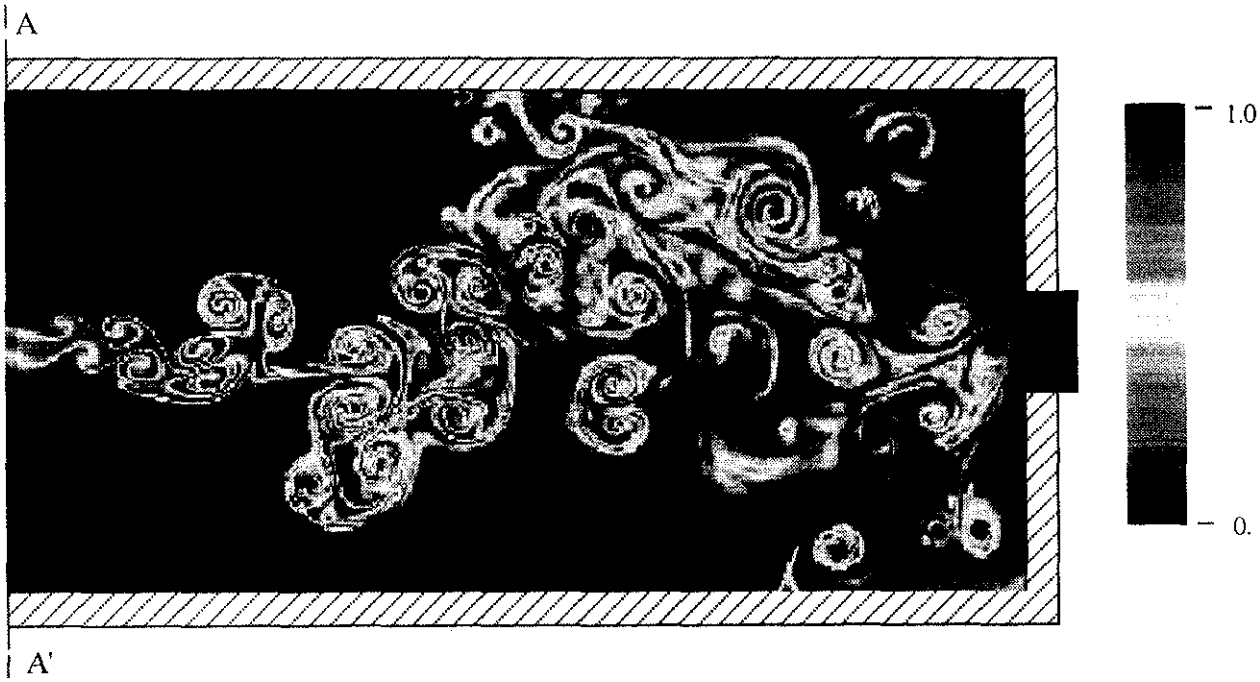

Fig. 4. Conserved scalar (ζ) field for ReSc=5000

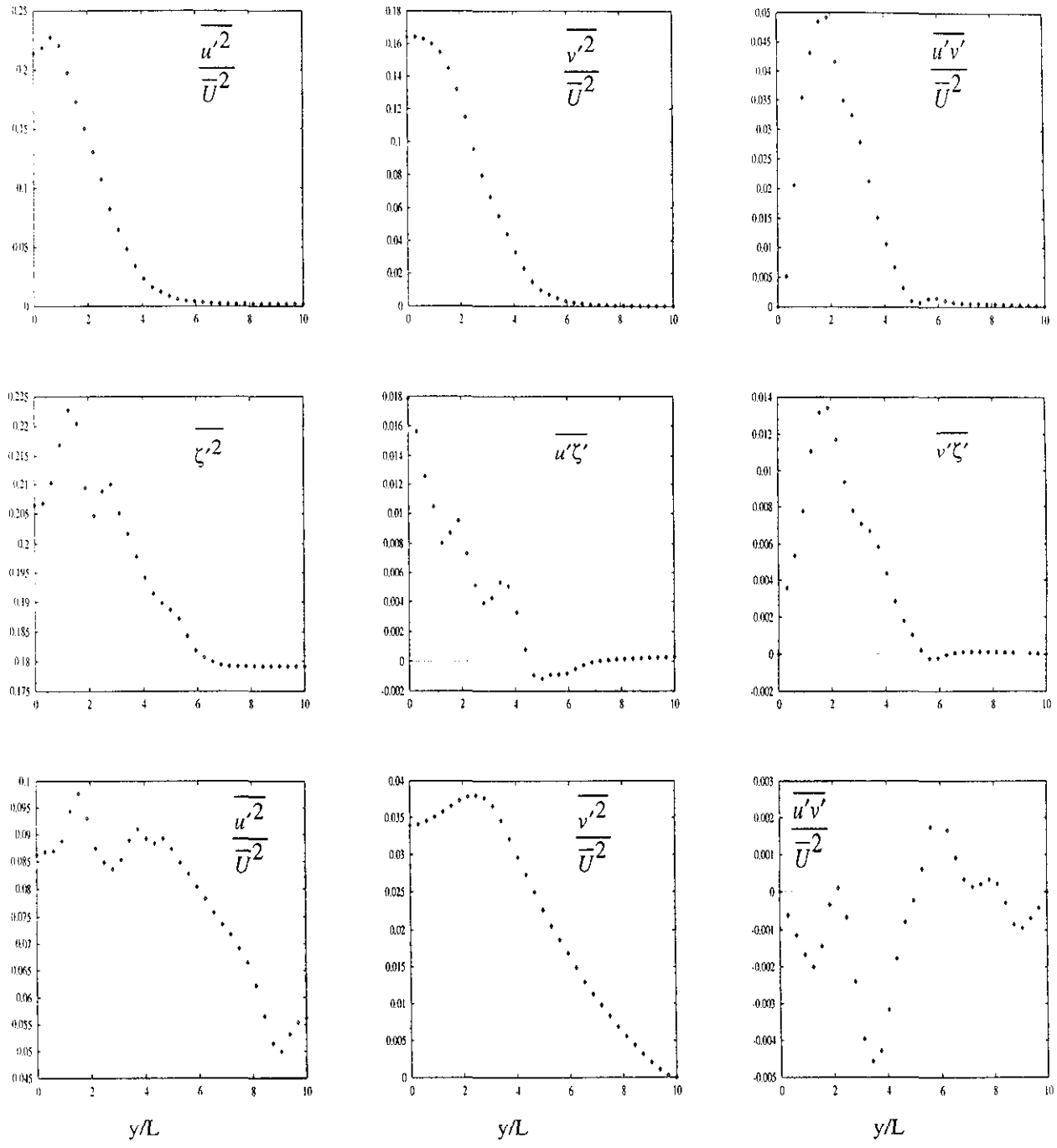

Fig. 5. Momentum flux profiles (top) and scalar flux profile (center) at location x/L=20; momentum flux profiles (bottom) at location x/L=35 of the 2-D jet.

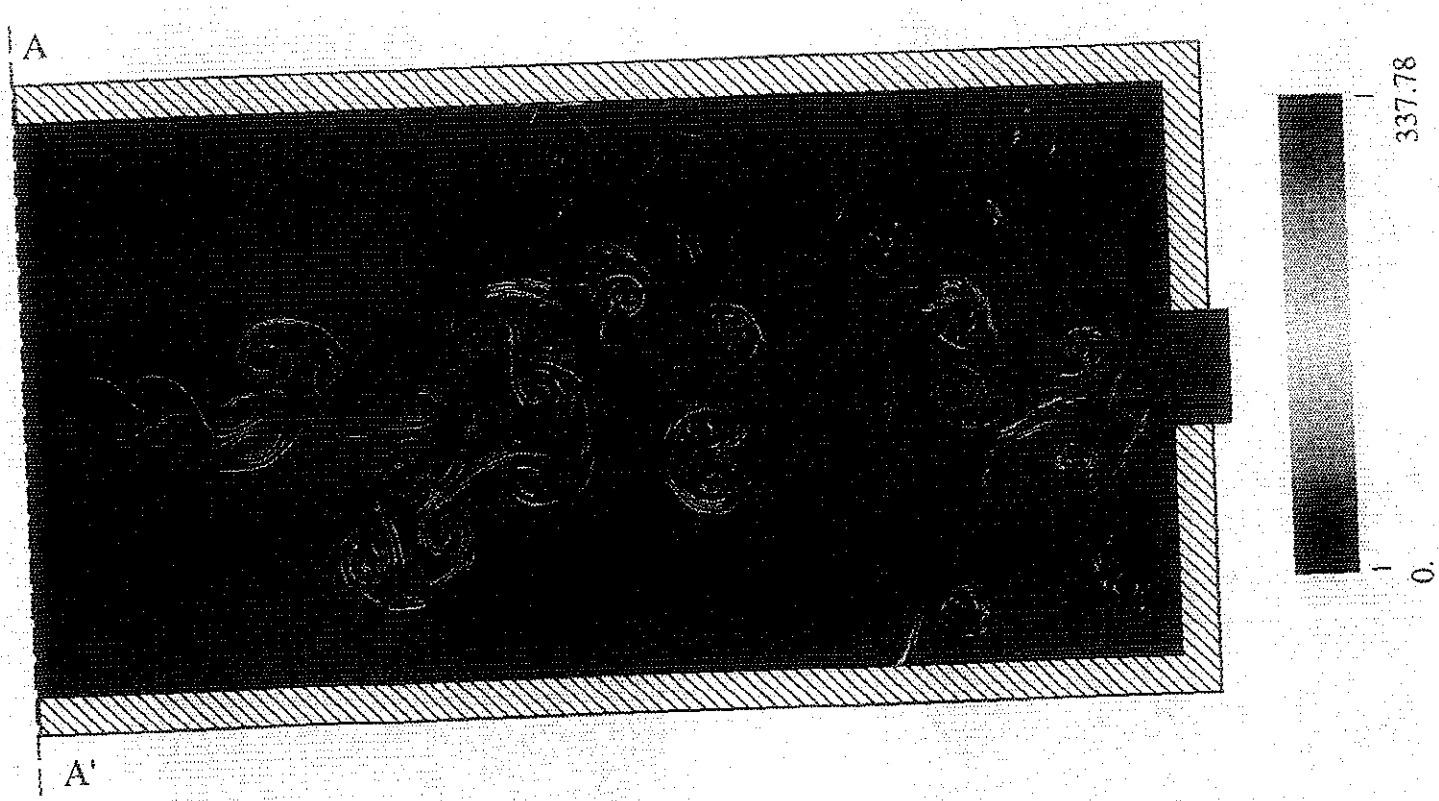

Fig. 6. Conserved scalar dissipation rate (χ) field for ReSc=5000

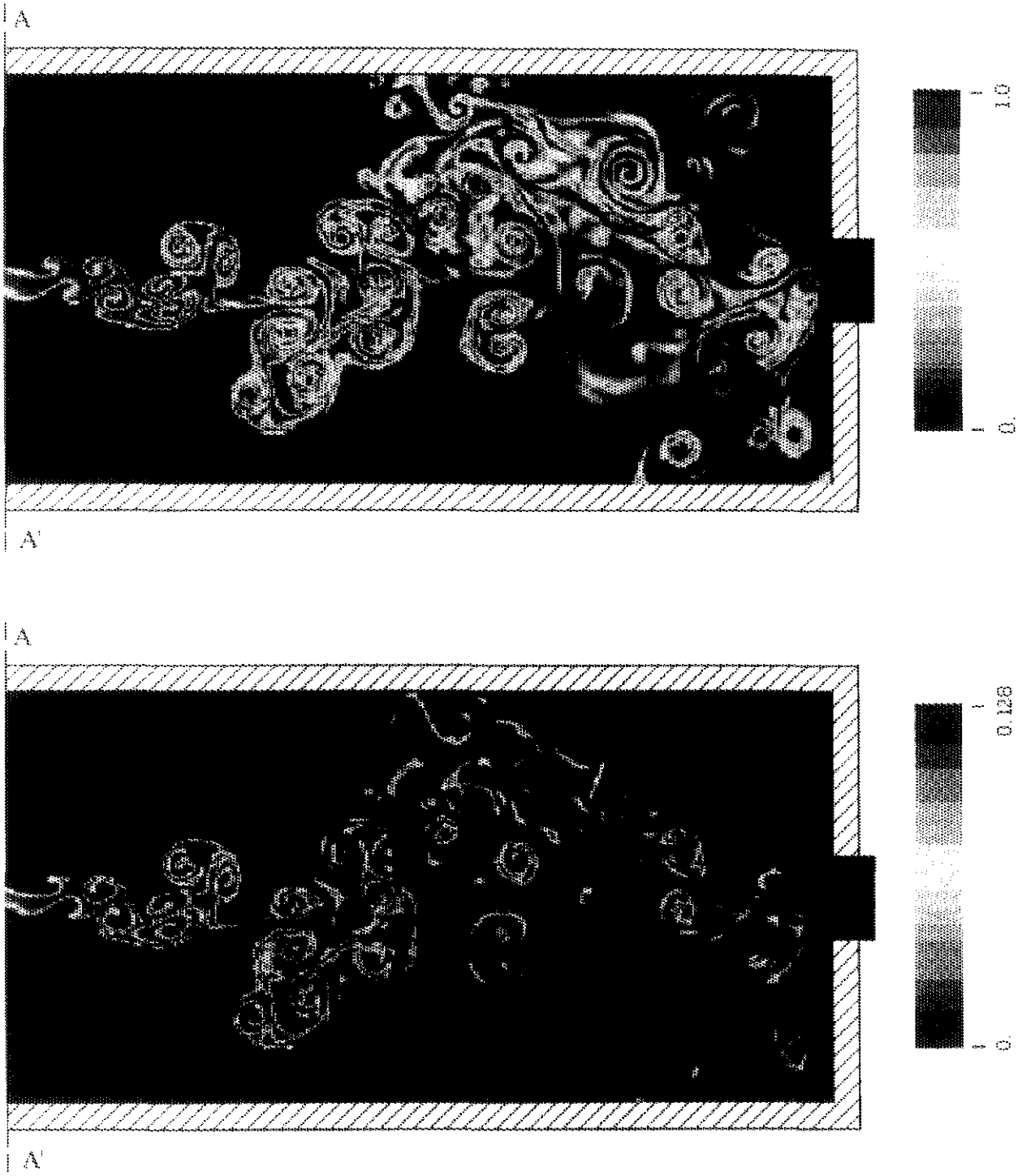

Fig. 7. CH_4 concentration field (moles/cc) (top - non-premixed flame with ReSc=500000; bottom-premixed flame with ReSc=50000).

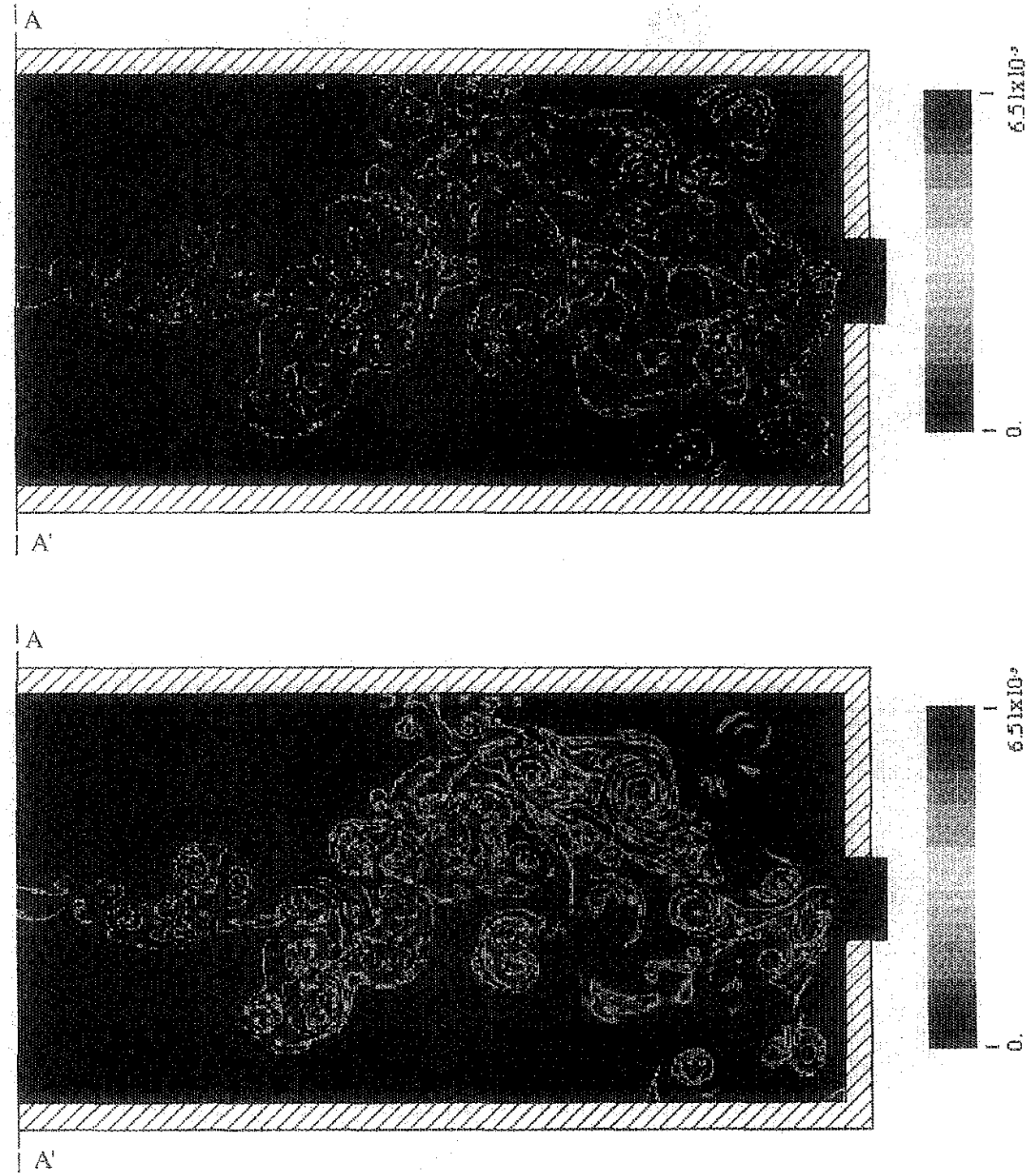

Fig. 8. OH concentration field (moles/cc) (top - non-premixed flame with ReSc=500000; bottom-premixed flame with ReSc=50000).

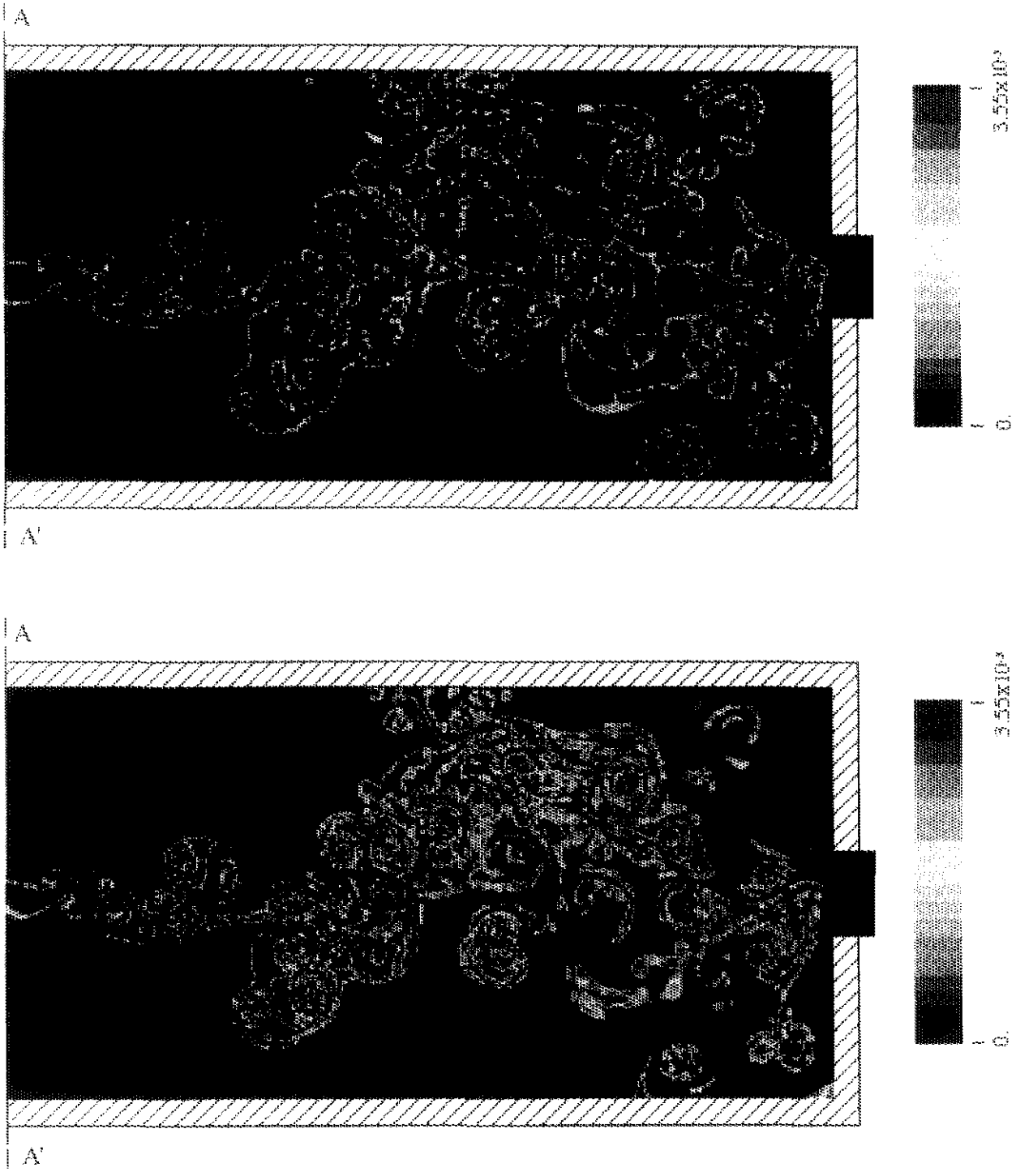

Fig. 9. O concentration field (moles/cc) (top - non-premixed flame with ReSc=500000; bottom-premixed flame with ReSc=50000).

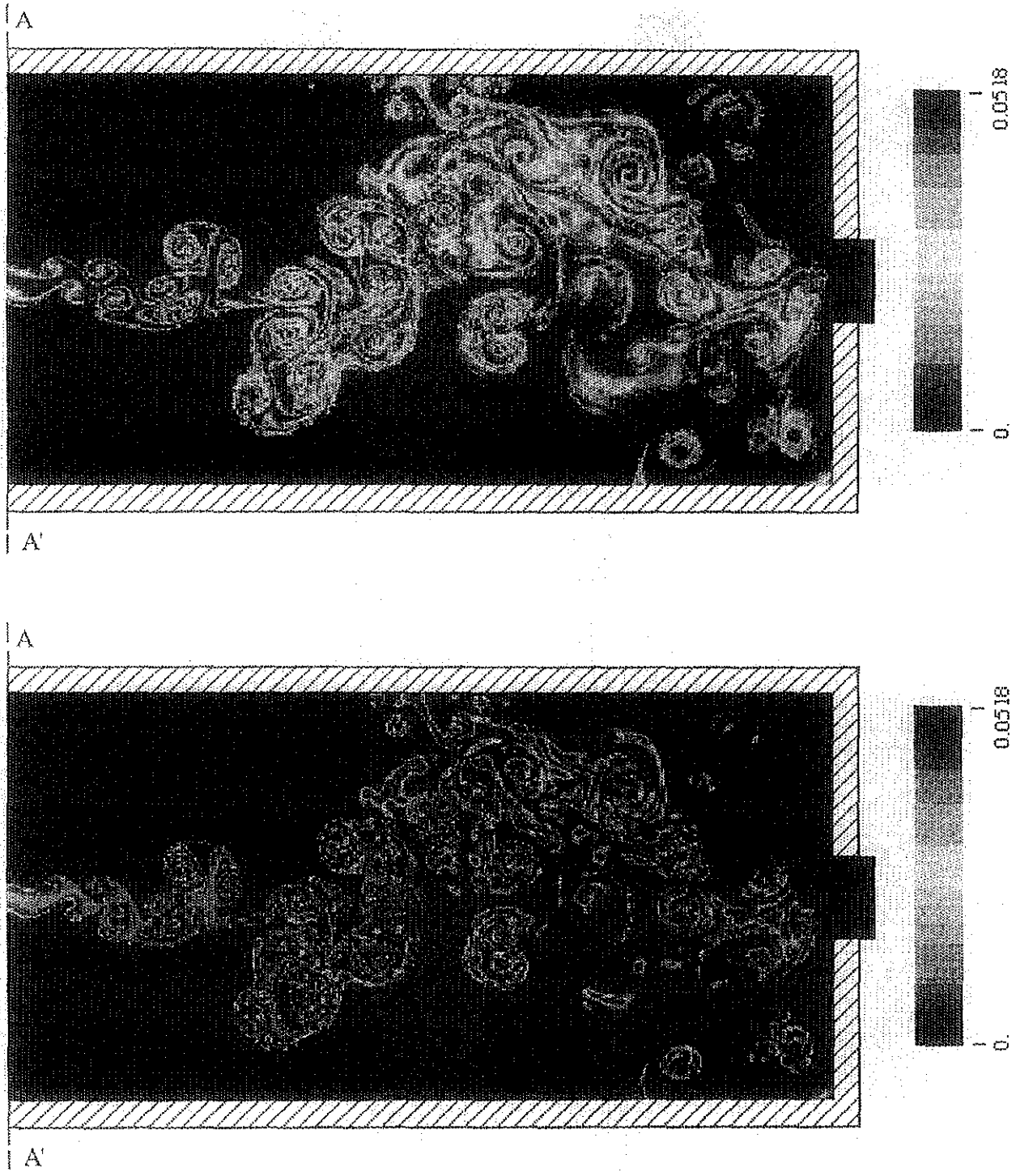

Fig. 10. CO concentration field (moles/cc) (top - non-premixed flame with ReSc=500000; bottom-premixed flame with ReSc=50000).

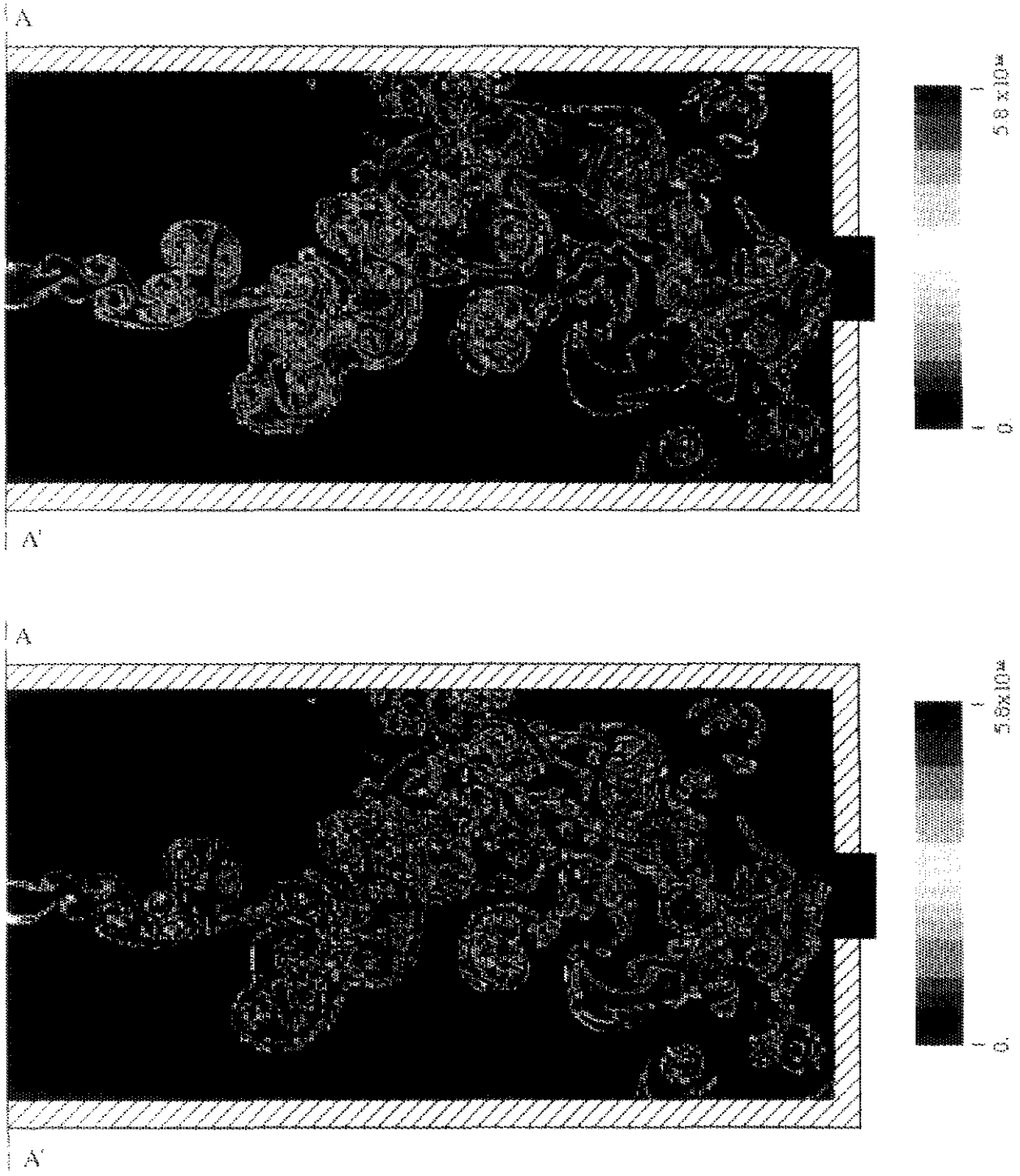

Fig. 11. $\nabla T \cdot \nabla T$ concentration field (K^2 / cm^2) (top - non-premixed flame with ReSc=500000, bottom - Premixed flame with ReSc=50000).